

# Sensitivity of Ionospheric Specifications to In Situ Plasma Density Observations Obtained From Electrostatic Analyzers Onboard of a Constellation of Small Satellites

Richard Balthazor, Matthew G. McHarg, C. Lon Enloe, Austin J. Wallerstein, Kody A. Wilson, Benjamin Rinaldi, Robert Raynor  
Space Physics and Atmospheric Research Center,  
Department of Physics  
United States Air Force Academy  
CO 80840  
719 333 4231  
richard.balthazor.ctr@usafa.edu

Ludger Scherliess, Robert W. Schunk  
Center for Atmospheric and Space Sciences  
Utah State University  
Logan, UT

Robert Brown, David J. Barnhart  
Department of Astronautics  
United States Air Force Academy  
CO 80840

## ABSTRACT

Our ability to specify and forecast ionospheric dynamics and weather at low- and mid-latitudes is strongly limited by our current understanding of the coupling processes in the ionosphere-thermosphere system and the coupling between the high and low latitude regions. Furthermore only a limited number of observations are available for a specification of ionospheric dynamics and weather at these latitudes. As shown by meteorologists and oceanographers, the best specification and weather models are physics-based data assimilation models that combine the observational data with our understanding of the physics of the environment. Through simulation experiments these models can also be used to study the sensitivity of the specification accuracy on different arrangements of observation platforms and observation geometries and can provide important information for the planning of future missions. For example, these studies can provide information about the number of spacecraft needed to improve the specification or evaluate the impact of different observation geometries on the accuracy of the specification. Here we have used the Global Assimilation of Ionospheric Measurements Full-Physics model (GAIM-FP) to study the sensitivity of ionospheric specifications on in situ plasma density observations obtained from electrostatic analyzers (ESA) onboard of a constellation of small satellites. The model is based on an Ensemble Kalman filter technique and a physics-based model of the ionosphere/plasmasphere (IPM), which covers the altitude range from 90 to 20,000 km. The data assimilation model can, in addition to the ESA observations, assimilate bottom-side  $N_e$  profiles from ionosondes, slant TEC from ground-based GPS stations, in situ  $N_e$  from DMSP satellites, occultation data from several satellites, and line-of-sight UV emissions measured by satellites. Simulation studies have been performed using various ESA constellation arrangements and their impact on the ionospheric specification has been evaluated. The results from this study will be presented with an emphasis on the number of satellites and their orbital geometries needed to improve ionospheric specifications and forecasts.

## INTRODUCTION

In recent years, there has been proposed space sensor networks [1-5] designed to cover selected orbits in LEO with either

- i) low-cost redundant “disposable” spacecraft-as-sensor platforms of CubeSat 1U size or smaller , or
- ii) low-cost low-SWAP sensors designed to be placed on as many conventional satellites as possible.

The primary objective of these missions is to provide a dense set of sensor data parameters to “fill in the gaps” of the relatively sparse coverage afforded by conventional multi-million-dollar missions [6] which produce single-point in-situ measurements.

Despite the lower cost of small satellites, low-SWAP instrumentation, and satellite-as-sensor hardware, a key question asked by funders is still “how many satellites/sensors are enough?”. What has become apparent is that there is no generally agreed metric for determining this question, and we attempt to bound the problem in this paper.

## SPACE WEATHER OBSERVATIONS

One area where the relative paucity of in-situ observations is notable is space weather. Figure 1 shows the rich expanse of observations available to terrestrial weather forecast models. (Nevertheless it is still notable that there are large data-gaps that directly affect the quality of weather forecasting.)

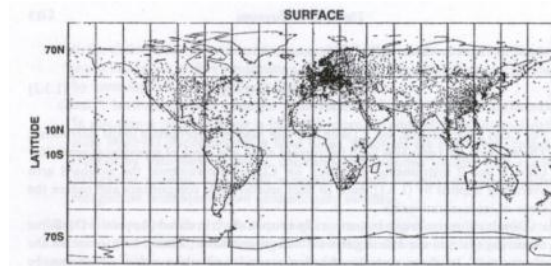


**Figure 1: Tropospheric in-situ weather measurement stations (Daley, Atmospheric Data Analysis, Cambridge University Press, 1991)**

Figure 2 shows, by comparison, typical weather measurement stations for space weather observations. What is immediately apparent is, similar to terrestrial weather in-situ sites in Figure 1, there is a paucity of measurements over the oceans and in remote continents. It should be noted that here, by contrast to the terrestrial weather case, the point-sources on the map are GPS/TEC remote measurements rather than in-

situ measurements. In addition, there are very much fewer space weather “stations” compared to the terrestrial weather case.

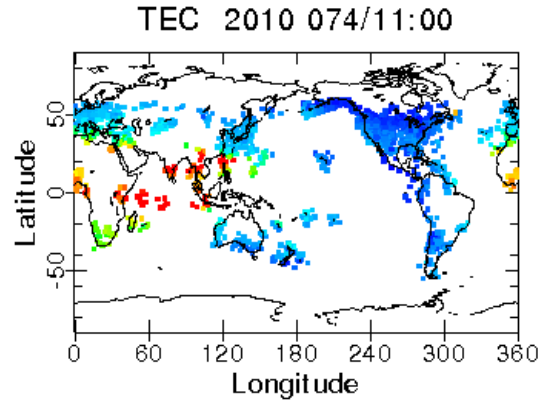


**Figure 2: Space weather remote measurements showing GPS TEC (slant TECs remapped to vertical). These measurements define the input to the GAIM global assimilative ionospheric model.**

The physics of the thermosphere and ionosphere varies over a wide range of scale sizes, from the ion and electron gyro-radii on the order of centimeters to large-scale global effects of the order of thousands of kilometers. While global scale phenomena have been studied since the 1930s, it is only recently that the importance of small scale phenomena to the energy budget of the coupled tropospheric - thermospheric - ionospheric - plasmaspheric system has been realized. Small scale (meters to hundreds of km) effects can be observed with spacecraft passing periodically through the region of interest, or by specialized remote techniques that effectively integrate over a small region of space and time. With LEO orbital parameters such that a single satellite only returns to the same position in space every ~97 minutes in the best case (and is then limited in the range of solar times it can observe), it is evident that more coverage (= more satellites) are required to provide in-situ coverage down to the small scale sizes and shorter temporal events of interest. The question here is how many satellites is enough?

We focus here on the thermosphere / ionosphere system. However, simultaneous observations (in-situ or remote sensing) from multiple similar satellites/sensors can be used for many applications – remote sensing (treaty sentinels, military applications, disaster monitoring), magnetosphere observations, solar wind measurements, pollution monitoring, and communications research, are but a few other examples.

## DESIGN REFERENCE SCENARIOS

The decadal research strategy, “The Sun to the Earth—and Beyond”, authored by the National Research Council [7] asks “*What specific physical processes transfer energy from the solar wind to geospace?*” In furtherance of this and other questions, it lists as its second priority the establishment of networks of satellites for radiation belt and ionospheric mapping. Additionally this study emphasizes the importance of “...*highly miniaturized sensors of charged and neutral particles...*” as well as calling for the gathering and assimilation of data from multiple platforms to “...*resolve spatial and temporal scales that dominate physical processes.*”

Accordingly we have compiled several design reference Scenarios for a satellite-as-a-sensor investigating and reporting back basic ionospheric parameters (density and temperature). Each Scenario is designed around both a primary and a secondary science objective. The primary science objective in each case is to provide measurements of plasma density and temperature to provide another input source for the USU Global Assimilation of Ionospheric Measurements (GAIM) model. The Scenarios have been chosen to illustrate the wide variety of possible secondary science and technical objectives. In each case we briefly discuss the science and technical objectives of the mission. For selected Scenarios we also investigate the effects on the GAIM model of introducing “data” from these satellite-sensors.

We have selected the two day period 13<sup>th</sup> - 15<sup>th</sup> March 2010 for our orbital scenario. This is because we happen to have continuous plasma density and temperature data for this period from i) the TEC inputs to GAIM, and ii) the MESA instrument on the MISSE7 experiment that flew on the International Space Station from November 2009 through May 2011.

### *Conceptual Satellite*

The concept of a satellite-as-a-sensor has been discussed before [3], where a new class of distributed space missions requiring simultaneous (in-situ or remote sensing) observations are assimilated to create multidimensional models. The concept was to deploy 10-100 satellites in a 500 km, 30 degree orbit, leveraging small ballistic coefficients between individual satellites to deploy them along a “string of pearls” configuration. It should be emphasized that this is not “formation flying” – indeed, there is no attitude or orbital adjust mechanism onboard each satellite (unlike, e.g., the Cluster constellation). Each satellite, a 1/4U CubeSat configuration, would use an ad-hoc mesh network or repeater network to communicate

ultimately to a dedicated downlink relay node. The lifetime would be short (~months) due to the low mass of each satellite. Unit costs would be low (as low as a few thousand dollars in 2007 prices), allowing a “disposable” mentality due to short lifetime and high redundancy. Barnhart demonstrated the viability of such a satellite-as-sensor, and this paper builds on that framework.

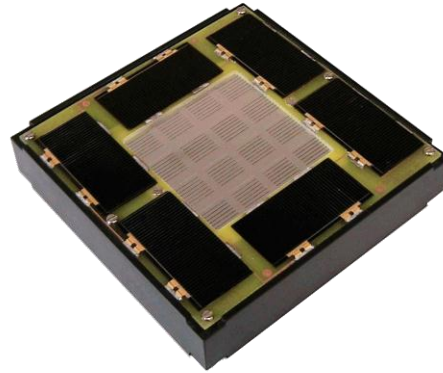


**Figure 3: Barnhart satellite-as-sensor prototype model, with electron-sensing MESA instrument face in the center of the solar panels.**

In each Scenario we assume a constellation of satellite-as-sensor devices based around the United States Air Force Academy MESA (Miniaturized Electrostatic Analyzer) [8] instrument built into a 1U CubeSat design. Although [3] demonstrated the viability of a 1/4U sensor enabling 12 satellites to be packed into a standard 3U P-POD launcher, currently available mesh network radios limit communication to ~100 km range, restricting the lifetime to a few days and in most cases before the evenly-spaced “string of pearls” configuration has been achieved.

Upsizing to a 1U design allows increase in available power by a factor of ~3.5, allowing each instrument to communicate to a ground station, network of ground stations, or space-based communications, independently and thus allowing a full evenly-spaced “string of pearls” configuration to downlink data without having to rely on the ad-hoc mesh network and a single download point. All of the constellation configurations presented later in this paper are ideally suited for direct downlinks, versus the mesh network architecture proposed for missions where small ionospheric features are of interest (1 - 100 km). However, with constellations of 10 satellites, managing the ground station can be an arduous task. Automation

is absolutely essential for these classes of missions, as most research institutions cannot afford a standing army of ground station crews working around the clock. An alternate approach, being pursued in the upcoming TechEdSat CubeSat mission, would be for each CubeSat to relay data through the ORBCOMM or IRIDIUM constellation. [9]

The idea of massively distributed constellations has caught on. The European QB50 effort has prompted various mission types, including space weather. One of the key benefits of these larger scale CubeSat missions is that it leverages economies of scale. As previously reported in [1] and updated in [2] the one-off costs of a CubeSat supporting a space weather mission are still in the \$90,000 range in 2012. However, the recent CubeSat trend has been to standardize on a 3U form factor to maximize power, but immediately imposes a 300% cost penalty per satellite sensor node. Table 1 below shows the unit cost and costs for a lot of 1000. For the purposes of this paper, a constellation size of 10 would yield a CubeSat cost of \$75,000 each.

**Primary Science Objective**

The primary science objective in all seven reference missions is to produce global maps of ionospheric data (plasma density and temperature) to ingest into an assimilative global ionospheric model.

**Sensing Instrument**

MESA (Figure 4) is a compact low-SWAP detector whereby charged particles (ions or electrons) enter an

offset chamber (Figure 5) through a grounded collimation slit and are deflected by a saddle electric field created by a biased plate. The voltage required to steer charged particles of energy  $E$  through a second grounded collimator offset from the first is approximately  $E$  (in eV)/1.6; that is, it takes ~10V to steer 16 eV particles through the device. The particles are steered through a double S-turn by a mirrored second biased plate set and third grounded exit collimator, and impinge upon an anode. The resultant current is measured by a transimpedance amplifier and the output voltage (proportional to current and hence charged particle density) digitized. The deflection voltage is swept and the detected signal at each step measured, to produce a charged particle energy spectra convoluted with the instrument response function, which is a well-characterizable Gaussian response. The sweeps are at 10 Hz, yielding a spatial resolution of ~750 m in LEO.

Measuring ions in LEO with MESA requires that the instrument be 3-axis stabilized and pointed into the ambient ram direction to within +/-4 degrees in pitch and yaw. However, this restriction goes away when the instrument measures only electrons, which can be collected in any attitude (and the ion density can then be estimated by assuming quasi-neutrality of the ambient plasma). Thus, the satellite-as-sensor can be a tumbler collecting electrons only.

The MESA instrument has flown to date on seven satellites in both ion- and electron-measuring modes, most recently returning data from the International

**Table 1. COTS CubeSat Configuration and Costs [2]**

\*approximate non-binding costs from vendors \*\*extrapolated cost by author

Subsystem	Vendor	Model	Mass (g)	Unit Cost @ 1	Unit Cost @1000
Payload	USAFA	MESA	130	\$2,763*	\$1,517**
Structure	Pumpkin	Skeletonized	155	\$1,350*	\$810*
EPS	Clyde Space	CubeSat EPS	310	\$25,240*	\$19,252*
DH	Pumpkin	FM430	90	\$1,200*	\$720*
Comm	Digi	XTend	18	\$179*	\$90*
ADCS	-	bar magnet	25	-	-
GPS	SSTL	SGR-05	20	\$20,000*	\$6,000**
Propulsion	None	-	-	-	-
Launch	CubeSat	Dnepr	-	\$40,000*	\$20,000**
<b>TOTALS:</b>			<b>748</b>	<b>\$90,732</b>	<b>\$48,389</b>
Comm	ISIS	UHF/VHF	120	\$25,600*	\$15,360**
<b>TOTALS:</b>			<b>738</b>	<b>\$116,332</b>	<b>\$63,749</b>

Space Station. It has flown with form factors as small as 1.5" diameter, although typically it is a package ~10 x 10 x 2.5 cm, operating from nominally 28V unregulated power. Typical power consumption is less than 1W, and the instrument stores up to 1 Gbyte of data onboard for later download. Communication is command/response via a RS-422 bus. Figure 4 shows the configuration of the MISSE-7 IMESA (Integrated MESA) flown onboard the ISS from November 2009 to May 2011. The above considerations, together with the low SWAP and flexible form factor makes it eminently suitable to be the primary payload on a 1-U CubeSat.

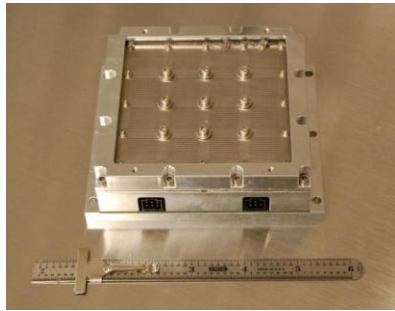


**Figure 4: MESA instrument flown onboard MISSE7, International Space Station, prior to launch.**

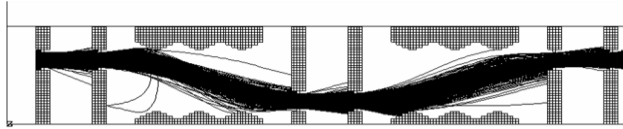


**Figure 5: SIMION cross-section of ion detection chamber. Ions (trajectories shown as black traces) enter at the left and are collimated by a pair of narrow slits. The ions then enter a deflection chamber (with scalloped edges) and are deflected through an S-turn through a second set of collimating plates. They then enter a second deflection chamber, reversing their S-turn, before exiting through a third set of collimating plates and impinge on an anode (not shown on right of image).**

**Scenario #1**

The first Scenario studied consists of ten satellites evenly distributed (string of pearls configuration) around a 500 km, 50 degree inclination orbit, with the orbital plane at 90 degrees longitudinal separation to the ISS orbital plane. 500 km altitude is chosen to be comfortably above the ISS orbit (to minimize the danger from space debris during the majority of the satellite operations) and to result in a lifetime well within the 25 years mandated by international treaty – the lifetime for a typical 1U CubeSat, 1 kg

satellite/sensor would be of the order of four years from 500 km at Solar minimum and 1.5 years from 500 km at Solar maximum.

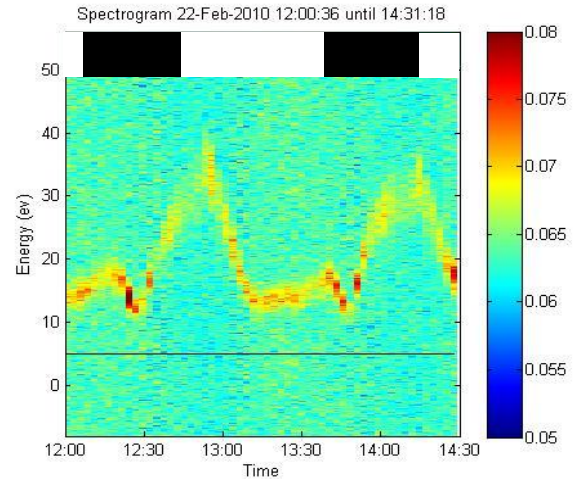


**Figure 6: Electron/ion spectrogram obtained from MESA instrument on MISSE7 onboard the ISS. Time runs along the horizontal axis, energy runs up the vertical axis, and the horizontal black line shows the expected response assuming zero ISS spacecraft charging. The white and black regions at the top of the plot indicate day and night respectively. The color scale is (currently uncalibrated) ion/electron density, and temperature may be obtained by determining the width of each spectra.**

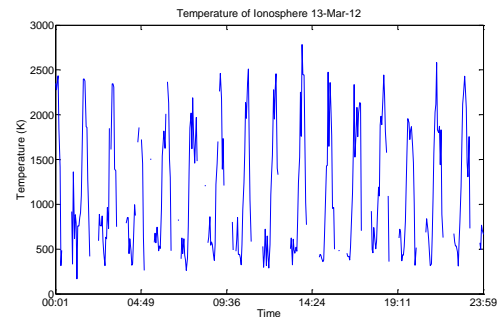


**Figure 7: Ion temperature as measured by IMESA onboard MISSE-7 over a 24 hour period on 13 March 2010. Temperatures cycle periodically as the ISS passes in and out of daylight. The lower temperature limit is unrealistically low, possibly as a result of an overly broad instrument response function. This is under investigation.**

The secondary objective of such a mission might be investigation of plasma bubbles in the low-latitude

ionosphere. A plasma bubble is an anisotropy in the equatorial ionosphere, caused primarily by the Generalized Rayleigh-Taylor instability [10] whereby perturbation electric fields crossed with the ambient magnetic field produce vertical amplitude growth. The net effect is to produce plasma depletions, ranging in size from a few cm to hundreds of km, rising in the equatorial ionosphere and propagating poleward along the Earth's magnetic field lines. These plasma depletions (or "bubbles") change the refractive index of the ionosphere and can scintillate radio signals used for communication and navigation. Thus, being able to nowcast and forecast such events is of prime interest to space systems operators. The Communication/Navigation Outage Forecasting System, C/NOFS, is an AFRL satellite designed to forecast radio and GPS scintillations [6]. However, the orbital inclination is only 13°, restricting visibility of plasma bubbles to low latitudes. Scenario #1 enables visibility of plasma bubbles as they disperse up to higher latitudes.

Although we have set the reference mission and primary science objective in the latter part of the mission lifetime when all ten satellites have evenly dispersed, valuable science data will be obtained all the way from post-launch when the satellites are spaced closer together. Plasma bubble scale sizes are thought to be down to centimeters, so (given a sufficiently high data-taking cadence) space-time ambiguities inherent with a single sensor can be resolved by comparing data from successive entries into/exits from plasma bubbles.

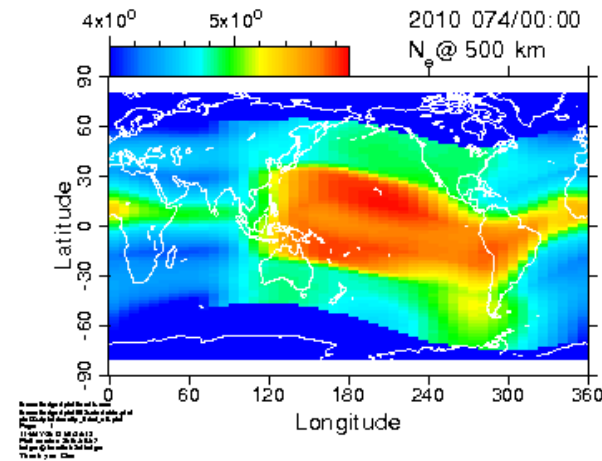


**Figure 8: Ionospheric density at 500 km from GAIM model. Note the higher densities in daylight and either side of the equator – the equatorial anomaly.**

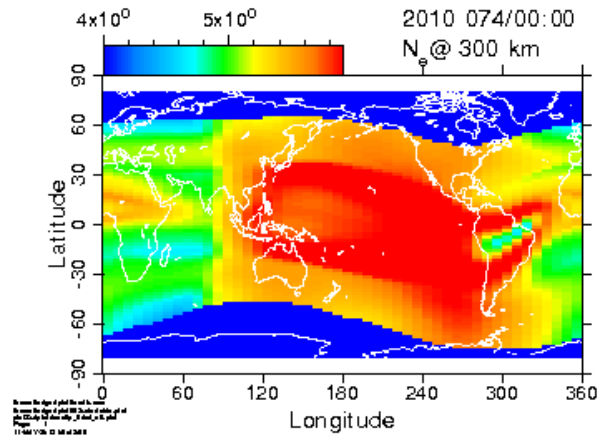


**Figure 9: As per Figure 8, but at 300 km.**

**Scenario #2a**

Ten satellites evenly distributed (string of pearls configuration) around a 500 km, 90 degree inclination orbit.

**Scenario #2b**

Ten satellites evenly distributed (string of pearls configuration) around a 350 km, 90 degree inclination orbit.

In contrast to investigating mainly low-latitude plasma bubbles in Scenario #1, this space sensor network would have the secondary objective of investigating high latitude phenomena such as the auroral regions, the cusp, and the polar cap. Again, significant use can be made of the sensor network during its “bunched” phase, studying plasma features with small scale sizes such as auroral arcs (few km) and the ionospheric Alfvén Resonator (IAR).

One aspect of understanding energy flow in the coupled magnetosphere – ionosphere system is understanding the role of low frequency plasma waves in driving ion outflow from the ionosphere to the magnetosphere. Recently, attention has fallen on the Ionospheric Alfvén Resonator (IAR) ([11] and references therein). The IAR is a cavity-resonator with natural frequencies ~0.1 - 5 Hz in the upper atmosphere, formed with a lower boundary at the conducting E-region and an upper boundary at the Alfvén speed maxima at around 1 RE. This cavity resonator is believed to play an important part in the development of perpendicular density and field aligned current (FAC) scales, resonant coupling with electromagnetic ion cyclotron waves that provide loss mechanisms for energetic particles in the radiation belt,

and ion and energy outflow feedback mechanisms into the ionosphere. However, the simultaneous multi-point in-situ observations inside the IAR cavity that are needed to categorize observationally how the waves and density structures evolve have never been made. The proposed sensor network will potentially lead to closure on these and other important science questions.

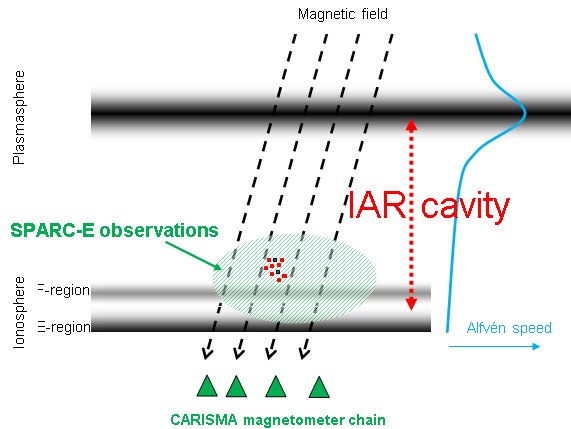


**Figure 10: Schematic of Ionospheric Alfvén Resonator cavity and observational regions of interest. The small squares represent sensor satellites in the early orbit (bunched) configuration.**

A range of plasma measurements is desirable:

- (i) Electron plasma density [est.  $10^{10}$ - $10^{12}$   $m^{-3}$ ]
- (ii) Ion and electron temperatures
- (iii) Transverse electric field [est.  $<200$  mV/m] and parallel electric field [est.  $<10$  mV/m]
- (iv) Transverse wave magnetic field [est.  $<10^{-6}$  T]
- (v) Three-dimensional ion flow velocity vector [est. 0.01-10 km/s]

Note that density and temperature measurements alone can be used with ground-based magnetometer measurements and other ground-based observations to specify parameters of the wave model for the IAR, and thus the complete set of plasma measurements (iii) – (iv) is not necessary to provide closure on processes excited by IAR wavemodes.

Remote imaging techniques integrate over the ionosphere within volumes that have scale sizes of several tens of km, and are thus unsuitable for determining the smaller spatial scales that are proposed in this study. Sensors on a single satellite taking point measurements suffer from an inherent inability to distinguish spatial and temporal effects, which is a

strong requirement for unambiguously studying waves. Inter-satellite separations increase over the lifetime of the mission from a few cm to tens of km. Complementing satellite observations, the characteristics of IAR and Pc1 ULF wave power on the ground will be provided primarily by data from the CARISMA array [12]. Cross-correlations of MESA density modulations and CARISMA field-aligned transport parameters will be used to look for evidence of IAR wave structures and their interaction with the lower boundary region.

### Scenario #3:

As per mission #1, but with an additional sensor onboard the ISS. The primary technical objective of this mission is to determine the “value added” of a sensor onboard the ISS in addition to the constellation in Scenario #1.

### Scenario #4

As per mission #2a, but with an additional sensor onboard the ISS. The primary technical objective of this mission is to determine the “value added” of a sensor onboard the ISS in addition to the constellation in Scenario #1. By contrast with Scenario #3, the eleventh sensor is added in a significantly lower inclination orbit, limiting the benefit to the secondary science mission.

### Scenario #5

A 5/5/1 Walker constellation at 500 km, 60 degrees inclination. This gives the bare minimum number of satellites for full continuous Earth coverage over low- to mid-latitudes, requiring five separate launches (of five individual satellites) to obtain the desired orbital injections. (The Walker delta pattern notation of  $t/p/f$  is such that a total constellation of  $t$  satellites has  $p$  orbital planes with an equal number of satellites distributed evenly in each plane. All the orbital planes are assumed to be the same inclination. The  $f$  parameter is the relative spacing between satellites in

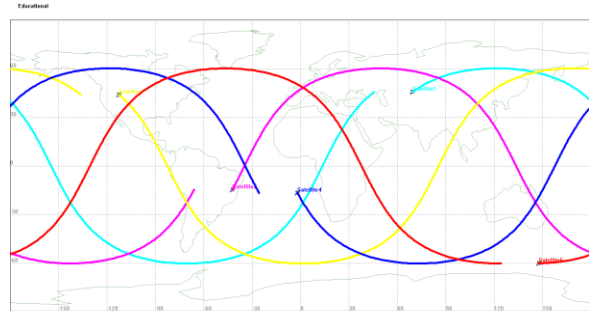


**Figure 11: Ground tracks of 60° inclination 5/5/1 Walker constellation**

adjacent orbital planes, such that the phase difference between a satellite at its ascending node and the adjacent satellite at the next most orbital plane to the east is given by  $360f/t$ .)

The primary science objective of this mission is benefited by the full Earth coverage, reducing data latency from the Scenario #1 case. For real-time forecasting, a data latency of less than two hours is ideal.

The secondary mission for such a constellation would be, once again, investigating plasma bubbles in the

ionosphere that cause radio scintillation. With global coverage now obtained, however (in contrast to Scenario #1), the opportunity arises for more detailed in-situ studies of plasma bubbles. Specifically investigations can be undergone of their evolution and life cycle. Increasing the number of satellites in each orbital plane, whilst outside the scope of the current paper, will increase the ability to resolve space-time ambiguities in the data and increase our knowledge of small-scale ionospheric perturbations known to play a part in plasma bubble formation and dynamics.

**Table 1 Design Scenario Orbital parameters summary**

Scenario	# of satellites	# of orbital planes	Inclination (degrees)	Altitude (km)	Inter-satellite separation <sup>**</sup> (km)	Secondary Mission
1	10	1	50	500	4100	Plasma bubbles
2a	10	1	90	500	4100	Ionospheric Alfvén Resonator
2b				350		
3	11	2	50 + 51.4	500	4100 <sup>‡</sup>	Plasma bubbles
4	11	2	90 + 51.4	500	4100 <sup>‡</sup>	Ionospheric Alfvén Resonator
5	5	5	60	500	n/a	Plasma bubble evolution
6	50	5	60	500	4100	
7	500	5	60	500	410	

\* Assumes evenly spread around orbit in string-of-pearls configuration

\*\* Between satellites in the same orbital plane

‡ Ignoring 11<sup>th</sup> sensor on ISS

**GENERATING MISSION DATA**

At Utah State University, we have developed two physics-based Kalman-filter data assimilation models for the Earth ionosphere. The two models are the Gauss-Markov Kalman Filter Model (GAIM-GM) and the Full Physics-Based Kalman Filter Model (GAIM-FP) [13-22] Both models are part of the Global

Assimilation of Ionospheric Measurements (GAIM) project. Some of the data that we have assimilated in our data assimilation models include in situ electron density measurements from DMSP satellites, bottomside electron density profiles from ionosondes, GPS-TEC data from a network of up to 1000 ground stations, ultraviolet (UV) radiances from the SSUSI, SSULI, and LORAAS instruments, and radio

occultation data from the CHAMP, SAC-C, IOX, and COSMIC satellites.

The Full Physics-Based Kalman filter model is based on an ensemble Kalman filter approach [23] and rigorously evolves the ionosphere and plasmasphere electron density field and its associated errors using a physics-based Ionosphere-Plasmasphere model (IPM) [13-15,24]. The IPM is based on a numerical solution of the ion and electron continuity and momentum equations [25] and covers the low and mid-latitudes from 90 to 30,000 km altitude. In its current version, the model excludes geomagnetic latitudes poleward of  $\approx \pm 60^\circ$  geomagnetic latitude due to the vastly different physical processes that govern the high-latitude regions, e.g. convection electric fields, particle precipitation, etc. The Full Physics-Based data assimilation model provides specifications on a spatial grid that can be global, regional, or local and its output includes the 3-dimensional electron and ion ( $\text{NO}^+$ ,  $\text{O}_2^+$ ,  $\text{N}_2^+$ ,  $\text{O}^+$ ,  $\text{H}^+$ ,  $\text{He}^+$ ) density distributions from 90 km to geosynchronous altitude (30,000 km). In addition, the model provides the self-consistent global distributions of the ionospheric drivers (electric field, neutral wind, and composition). It is important to note that the estimation of the ionospheric drivers is an integral part of our ensemble Kalman filter and is achieved by using the internal physics-based model sensitivities to the various driving forces. In this procedure, the ionospheric data are used to adjust the plasma densities and its drivers so that a consistency between the observations (within their errors) and the physical model is achieved. As a result the assimilation procedure produces the optimal model-data combination of the ionosphere-plasmasphere system with its self-consistent drivers (electric fields and neutral winds and composition) [26,27].

### ***Kalman Filter Simulations***

The Full Physics-Based data assimilation model is generally being used to specify ionospheric weather, but the model can also be used to study the sensitivity of the specification accuracy on different arrangements of observation platforms and observation geometries and can provide important information for the planning of future missions [28,29]. For the current study this latter mode has been used and simulation experiments have been performed. In this mode the model uses a Data Simulation System Experiment (OSSE) using two different synthetic (model-generated) data types: slant TEC from ground-based GPS stations and in situ electron density measurements from a variety of CubeSats in various orbital configurations. In the OSSE, the simulated weather (true) time-dependent ion and electron density distributions are generated by using again the IPM model. For these simulations we

varied the equatorial vertical drift and horizontal neutral winds by superposing on the climatology values a random component. Note that neither the climatological values nor the random components are known to the Kalman filter part. The synthetic data were then generated by probing the 3-D, time-dependent electron density distribution for the weather (true) simulation exactly the same way the real instruments probe the real ionosphere. For the GPS receivers, slant TEC values were generated only for elevation angles greater than  $15^\circ$ . For the in situ electron densities synthetic observations were generated in 10-sec increments. When the synthetic data were generated, noise was added to each "measurement" in order to mimic a real observation. A 5 TEC unit (TECU) level of noise was added to all simulated TEC measurements and a 10% uncertainty to the simulated in situ measurements.

The Kalman filter assimilation procedure was implemented as follows. At 1200 UT on day 2010/073 the plasma distribution obtained from the climatology run was taken to be the initial distribution at the start of the assimilation. Every 15 min, the evolving weather simulation was probed to obtain the two synthetic data types (with noise) as described above. At these time marks the ensemble of ionosphere/plasmasphere model runs was also integrated forward in time, and the model error covariance matrix was determined [27]. Using the new data and the new error matrix, the Kalman filter reconstructed an updated estimate of the plasma distribution and its drivers. The new drift and wind velocities were fed back into the IPM and the assimilation was repeated at the next 15 min time mark. As time advanced, the Kalman filter produced a 3-D, time-dependent, plasma distribution that got closer and closer to the 'true' plasma distribution associated with our weather simulation.

### **RESULTS**

In the following, we will show example results from our full physics-based data assimilation model. For these runs the model assimilated simulated slant TEC from a network of more than 150 GPS ground receivers and in situ plasma density observations from the satellite constellations outlined in Table 3. Furthermore in one of the model runs only GPS slant TEC data were assimilated (GPS-Only case), which we have used as a reference run. For all model runs the ionospheric plasma density and its drivers were specified on a global scale from  $\pm 60^\circ$  magnetic latitude. Clearly there are many ways how to compare the various model results and different applications will require different metrics. Here we will focus on the large-scale plasma density distribution with the main emphasis on Scenario 2a and 2b.

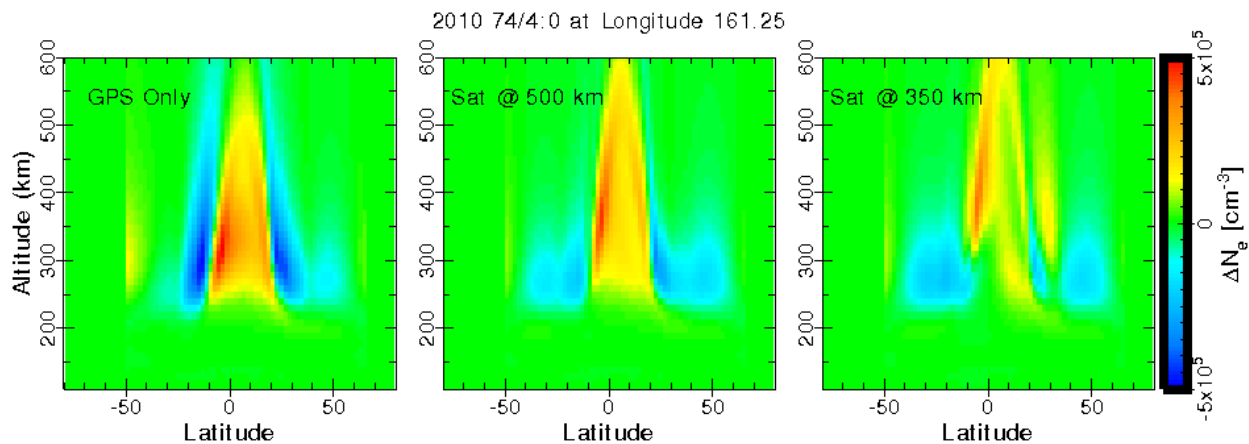
Figure 12 shows, as an example, a snapshot of the simulated global data distribution (top panel) for 04:00 UT on day 74 in 2010. The color-coded dots correspond to slant TEC values shown at their 300 km pierce point location. The two near-vertical lines represent the ground-track of the 10 satellites corresponding to Scenario 2a (10 satellites at 500 km altitude) during this time. The colors for these lines represent the in situ plasma densities at the satellite altitude (500 km) ranging from a value of zero (blue) to  $6 \cdot 10^5 \text{ cm}^{-3}$  (red). The bottom panel of Figure 12 shows the vertical TEC distribution obtained from the Kalman filter reconstruction after assimilating the slant TEC data together with the in situ plasma density measurements corresponding to the scenario shown in the top panel. The vertical TEC was obtained by integrating through the 3-D ionosphere-plasmasphere from 90 km to the upper boundary. Clearly seen is a hemispheric asymmetry during the daytime hours with larger TEC values in the southern hemisphere, the equatorial anomalies during the daytime hours separated from the magnetic equator by about  $10\text{-}15^\circ$  on both sides of the magnetic dip equator.

Figure 13 illustrates the improvements in the Kalman filter reconstructions associated with the assimilation of the in situ plasma densities. Shown are altitude-latitude cuts of the plasma residuals for the GPS-Only case (left panel), Scenario 2a (middle panel), and Scenario 2b (right panel). The plasma density residuals were calculated by subtracting from the 3-D ionosphere Kalman filter reconstructions the corresponding plasma densities from the Truth run with green indicating no difference, red overestimation, and blue underestimation. The residuals are shown for 04:00 UT on day 74 in 2010 and correspond to  $161.25^\circ$  longitude. This longitude is located over the Pacific Ocean with only sparse GPS data coverage and approximately aligns with the location of the in situ plasma density observations shown in Figure 12 (top panel). Note, that at this longitude, the magnetic equator is about  $10^\circ$  north of the geographic equator. Figure 13 shows that the Kalman filter reconstruction for the GPS-Only case overestimates the plasma densities at equatorial and low latitudes ( $\pm 15^\circ$  magnetic latitude) followed by an underestimation in the transition region from low to middle latitudes (near  $15\text{-}20^\circ$  magnetic latitude). Scenario 2a (middle panel) shows an overall reduction in the residual values when compared with the GPS-Only case with the largest improvements in the transition from low to middle latitudes. Scenario 2b (right panel) indicates an even more dramatic reduction in the overall residual values. Note that even though the in situ plasma densities correspond to fixed height, e.g., 350 and 500 km, the improvements in the Kalman filter results are not limited to these altitudes but instead

affect the entire plane as well as neighboring longitude sectors (not shown here).

To further illustrate the difference between the 3 model simulations and to show the impact of the in situ plasma density observations on the model performance, Figure 14 shows electron density profiles from 120 to 800 km altitude for the GPS-Only case (red), Scenario 2a (green), Scenario 2b (blue), and the Truth run (black). The profiles correspond again to 04:00 UT on day 74 in 2010 and to  $161.25^\circ$  longitude and  $10^\circ$  latitude (close to the magnetic dip equator). Clearly seen are large reductions in the errors of the F region electron density specifications when the satellite data were assimilated, with the largest improvements when the satellite data correspond to an altitude of 350 km. In particular is the error in the peak F region density  $N_m F_2$  significantly reduced from a value of about  $3 \cdot 10^5$  for the GPS-Only case to about  $1 \cdot 10^5$  for Scenario 2b. Similar improvements can also be seen in the width of the F layer.

Figure 15 shows latitude variation of the electron densities at 350 km altitude (bottom panel) and 500 km altitude (top panel) for the same 4 cases depicted in Figure 14. At 350 km altitude all three Kalman filter reconstructions show the development of the equatorial anomaly in agreement with the Truth run. However, the separation of the anomaly peaks and the peak-to-trough ratio exhibit significant differences. For the GPS-Only case the peaks are not separated enough and the peak-to-trough ratio is too small when compared to the Truth run. For scenario 2a (satellites at 500km) the peak to trough ratio is improved and the poleward edge of the anomaly is in good agreement with the Truth run. For scenario 2b (satellites at 350 km) both peak location and peak-to-trough ratio is found to be closest to the truth conditions. At 500 km altitude the situation is more complicated. At this altitude no overall improvements are seen when the satellite data are assimilated but certain aspects of the latitude profile show improvements. For example, the GPS-Only case lacks the development of clear equatorial anomalies at this altitude and the large gradients associated with the poleward edge of the anomaly occur too far equatorward. Both of these shortcomings are overcome by assimilating the in situ plasma densities. In particular is the poleward edge of the anomaly and its large gradients in good agreement with the truth run. The anomaly peaks, however appear too close to the magnetic equator and differ in magnitude from the Truth run by about 20-30%. Nevertheless, the build-up of the anomalies at this altitude indicates that the equatorial vertical drifts (zonal electric fields) determined by the Kalman filter are strong enough to lift the plasma from the lower altitudes high enough to



**Figure 13: Altitude-latitude cuts of the plasma density residuals for 04:00 UT on day 74 in 2010 and 161.25° geographic longitude for the GPS-Only case (left panel), Scenario 2a (middle panel), and Scenario 2b (right panel). The plasma density residuals were calculated by subtracting the plasma densities from the truth run from the corresponding 3-D ionosphere Kalman filter reconstructions.**

form the anomalies. As a result of this lift-up the peak-to-trough ratio at lower altitudes are enhanced and the poleward edge of the anomalies move poleward leading to the improvements seen at 350 km altitude. It is interesting to note that the Kalman filter reconstruction near the equator for scenario 2a (satellites at 500 km) differ significantly from the Truth run at 500 km altitude. One possible explanation for this discrepancy is the long time history (several hours) of uplift necessary to match the values at his altitude. The details of this time history, however, are only vaguely known to the Kalman filter due to a lack of prior satellite observations and the lack of sufficient nearby GPS ground receivers.

## CONCLUSION

Our model simulations have shown that adding a constellation of small satellites/sensors in addition to global TEC inputs does indeed converge the GAIM model closer to “truth” in the situations we describe, and this approach can be used to fine-tune initial orbital parameters to optimize the model inputs (for example, lowering the orbital altitude from 500 km to 350 km in Scenario #2(a,b) improves considerably the equatorial features of the GAIM model. (What is particularly interesting is that the model is improved over a range of altitudes, not just at and around the satellite/sensor altitude, emphasizing the coupled nature of both the model and reality, with plasma dynamics extending along magnetic flux tubes. Put another way, knowledge at one location leads to improved knowledge at other locations). However, what has become apparent is the challenge to develop a generally agreed metric to measure the scientific and operational benefit to assimilative models from the use of multiple small satellite/sensor inputs.

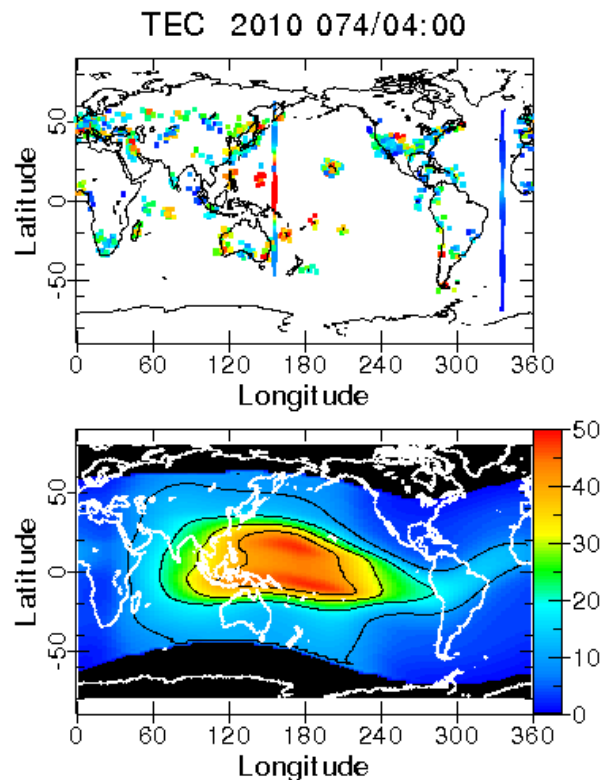


**Figure 12: Snapshot of the simulated global data distribution (top panel) for 04:00 UT on day 74 in 2010. The color-coded dots correspond to slant TEC values shown at their 300 km pierce point locations. The two near-vertical lines represent the ground-track of the 10 satellites corresponding to Scenario 2a (10 satellites at 500 km altitude) during this time. The color-code for these lines corresponds to the in situ plasma densities at the satellite altitude (500**

km) ranging from values of zero (blue) to  $6 \cdot 10^5 \text{ cm}^{-3}$  (red). The bottom panel of Figure 12 shows the vertical TEC distribution obtained from Kalman filter reconstruction after assimilating the slant TEC data together with the in situ plasma density measurements corresponding to the scenario shown in the top panel. The vertical TEC was obtained by integrating through the 3-D ionosphere-plasmasphere from 90 km to the upper boundary.

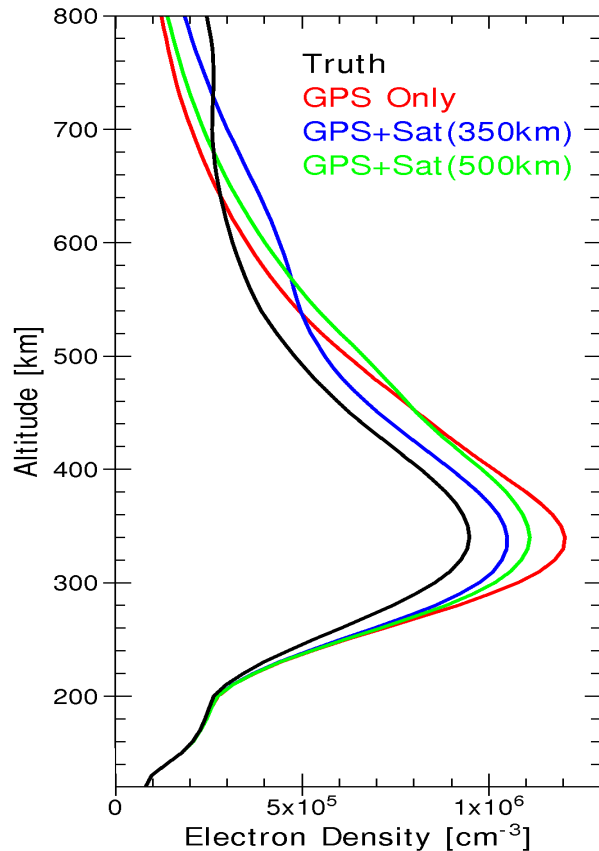


Figure 14: Electron density profiles from 120 to 800 km altitude for the GPS-Only case (red), Scenario 2a (green), Scenario 2b (blue), and the Truth run (black). The profiles correspond to 04:00 UT on day 74 in 2010 and to 161.25° longitude and 10° latitude.

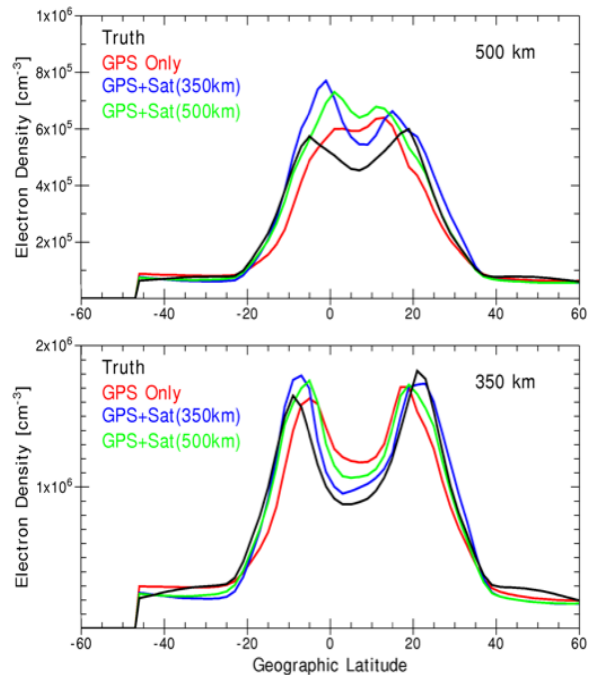


Figure 15. Latitude variation of electron densities for the GPS-Only case (red), Scenario 2a (green), Scenario 2b (blue), and the Truth run (black) at 500 km altitude (top panel) and 350 km altitude (bottom panel). The profiles correspond to 04:00 UT on day 74 in 2010 and to 161.25° geographic longitude.

## REFERENCES

1. Barnhart, D.J., T. Vladimirova and M.N. Sweeting, "Satellite Miniaturization Techniques for Space Sensor Networks", Journal of Spacecraft and Rockets, Vol 46, No. 2, March-April 2009, doi 10.2514/1.41639
2. Barnhart, D. J., "Very Small Satellites Design for Space Sensor Networks," Ph.D. Thesis, Univ. of Surrey, Guildford, England, U.K., June 2008, <http://handle.dtic.mil/100.2/ADA486188>
3. Barnhart, D. J., T. Vladimirova, M. N. Sweeting, R. L. Balthazor, C. L. Enloe, L. H. Krause, T. J. Lawrence, M. G. Mcharg, J. C. Lyke, J. J. White, and A. M. Baker, "Enabling Space Sensor Networks with PCBSat," AIAA Paper SSC07-IV-4, Aug. 2007.
4. T. Vladimirova, N. P. Bannister, J. Fothergill, G. W. Fraser, M. Lester, D. M. Wright, M. J. Pont, D. J. Barnhart, O. Emam, "CubeSat Mission for Space Weather Monitoring", Proceedings of 11th

- Australian Space Science Conference, ASSC'11, 26 - 29 September 2011, Canberra, Australia.
5. Barnhart, D. J., Vladimirova, T., and Sweeting, M. N., "Very Small Satellite Design for Distributed Space Missions," *Journal of Spacecraft and Rockets*, Vol. 44, No. 6, 2007, pp. 1294-1306.
  6. De la Beaujardiere, O., "C/NOFS: a Mission to Forecast Scintillations," *Journal of Atmospheric and Solar-Terrestrial Physics*, Vol. 66, No. 17, 2004, pp. 1573-1591.
  7. The Sun to the Earth—and beyond, a Decadal Research Strategy in Solar and Space Physics, Solar and Space Physics Survey Committee, National Research Council, the National Academies Press, ISBN 0-309-50800-2, 2003.
  8. <http://www.uk.amsat.org/5018>
  9. Enloe, C.L., L. Habash Krause, R. K. Haaland, T. T. Patterson, C. E. Richardson, C. C. Lazidis, and R. G. Whiting, "Miniaturized electrostatic analyzer manufactured using photolithographic etching", *Rev. Sci. Inst.*, Vol 74, No. 3, 2003
  10. Krause, L. H., C.L. Enloe, R.K. Haaland and P. Golando, "Microsatellite missions to conduct midlatitude studies of equatorial ionospheric plasma bubbles", *Advances in Space Research*, Vol 36, No. 12, 2005, pp2474-2479.
  11. Lysak, R. L., and A. Yoshikawa, "Resonant cavities and waveguides in the ionosphere and atmosphere", in *Magnetospheric ULF Waves*, K. Takahashi et al. (eds.), AGU Monograph Series, American Geophysical Union, Washington, p. 289, 2006.
  12. Mann, I. R., D.K. Milling, I.J. Rae, A. Kale, Z.C. Kale, K.R. Murphy, A. Parent, M. Usanova, D.M. Pahud, E.-A. Lee, V. Amalraj, D.D. Wallis, V. Angelopoulos, K.-H. Glassmeier, C.T. Russell, H.-U. Auster, and H.J. Singer, "The Upgraded CARISMA Magnetometer Array in the THEMIS Era", *Space Sci. Rev.*, Vol 141, 1-4, 2008, pp 413-451
  13. Schunk, R.W., L. Scherliess, J.J. Sojka, and D. Thompson (2004), Global Assimilation of Ionospheric Measurements (GAIM), *Radio Sci.*, 39, RS1S02, doi:10.1029/2002RS002794.
  14. Schunk, R.W., L. Scherliess, J.J. Sojka, D. Thompson, and L. Zhu (2005), Ionospheric Weather Forecasting on the Horizon, *Space Weather*, 3, S08007, doi:10.1029/2004SW000138.
  15. Scherliess, L., R.W. Schunk, J.J. Sojka, and D. Thompson (2004), Development of a Physics-Based Reduced State Kalman Filter for the Ionosphere, *Radio Sci.*, 39, RS1S04, doi:10.1029/2002RS002797.
  16. Scherliess, L., R.W. Schunk, J.J. Sojka, D.C. Thompson, and L. Zhu (2006), The USU GAIM Gauss-Markov Kalman Filter Model of the Ionosphere: Model Description and Validation, *J. Geophys. Res.*, 111, A11315, doi:10.1029/2006JA011712.
  17. McDonald, S. E., S. Basu, S. Basu, K.M. Groves, C.E. Valladares, L. Scherliess, D. Thompson, R. W. Schunk, J.J. Sojka and L. Zhu (2006), Extreme Longitudinal Variability of Plasma Structuring in the Equatorial Ionosphere on a magnetically quiet equinoctial day, *Radio Sci.*, 41, RS6S24, doi:10.1029/2005RS003366.
  18. Thompson, D.C., L. Scherliess, J.J. Sojka, R.W. Schunk (2006), The Utah State University Gauss-Markov Kalman Filter of the Ionosphere: The Effects of Slant TEC and Electron Density Profile Data on Model Fidelity, *J. Atmos. and Sol-Terr. Phys.*, doi:10.1016/j.jastp.2005.10.011.
  19. Thompson, D.C., L. Scherliess, J.J. Sojka, R.W. Schunk (2008), Upper Ionosphere Effects on the Assimilation of GPS Slant TEC, *Proceedings of the Ionospheric Effects Symposium*, (Ed. J.M. Goodman), JMG Space Associates.
  20. Sojka, J.J, D. Thompson, L. Scherliess, and R.W. Schunk (2007), Assessing Models for Ionospheric Weather Specification over Australia During the 2004 CAWSES Campaign, *J. Geophys. Res.*, 112, A09306, doi:10.1029/2006JA012048.
  21. Jee, G, A.G. Burns, W. Wang, S.C. Solomon, R.W. Schunk, L. Scherliess, D.C. Thompson, J.J. Sojka, and L.Zhu (2007), Duration of Ionospheric Data Assimilation Initialization of a Coupled Thermosphere-Ionosphere Model, *Space Weather Journal*, 5, S01004, doi:10.1029/2006SW000250.
  22. Jee, G, A.G. Burns, W. Wang, S.C. Solomon, R.W. Schunk, L. Scherliess, D.C. Thompson, J.J. Sojka, and L.Zhu (2008), Continual Initialization of the TING Model with GAIM Electron Densities: Ionospheric Effects on the Thermosphere, *J. Geophys. Res.*, 113, A03305, doi:10.1029/2007JA012580.
  23. Evensen, G. (2003), The Ensemble Kalman Filter: Theoretical Formulation and Practical

- Implementation, *Ocean Dynamics*, 53, 343–367, DOI 10.1007/s10236-003-0036-9.
24. Scherliess, L. D. Thompson, R.W. Schunk, and J.J. Sojka (2006b), Ionospheric/thermospheric variability at middle latitudes obtained from the global assimilation of ionospheric measurements (GAIM) model, *Eos Trans. AGU*, 87(52), Fall Meet. Suppl., Abstract SA12A-03.
  25. Schunk, R. W., and A. F. Nagy (2000), *Ionospheres*, Cambridge University Press, Cambridge, U.K..
  26. Scherliess, L., D.C. Thompson, and R.W. Schunk, 2009, Ionospheric dynamics and drivers obtained from a physics-based data assimilation model, *Radio Science*, 44, RS0A32, doi: 10.1029/2008RS004068.
  27. Scherliess, L., D.C. Thompson, and R.W. Schunk, 2011, Data assimilation models: A ‘new’ tool for ionosphere science and applications, in *The Dynamic Magnetosphere*, Springer, doi 10.1007/978-94-007-0501-2\_18.
  28. Atlas, Robert, 1997: Atmospheric observations and experiments to assess their usefulness in data assimilation. *JMSJ*, Vol. 75, pp. 111-130.
  29. Atlas, R., E. Kalnay, J. Susskind, W. E. Baker and M. Halem, 1985: Simulation studies of the impact of future observing systems on weather prediction. Proc. Seventh Conf. on NWP. 145-151.